Evaluating Weather Research and Forecasting (WRF) Model Predictions of Turbulent Flow Parameters in a Dry Convective Boundary Layer

JEREMY A. GIBBS AND EVGENI FEDOROVICH

School of Meteorology, University of Oklahoma, Norman, Oklahoma

ALEXANDER M. J. VAN EIJK

Netherlands Organisation for Applied Scientific Research (TNO), The Hague, Netherlands, and Laboratoire de Mecanique de Fluides UMR 6598 CNRS, Ecole Centrale de Nantes, Nantes, France

(Manuscript received 20 September 2010, in final form 29 July 2011)

ABSTRACT

Weather Research and Forecasting (WRF) model predictions using different boundary layer schemes and horizontal grid spacings were compared with observational and numerical large-eddy simulation data for conditions corresponding to a dry atmospheric convective boundary layer (CBL) over the southern Great Plains (SGP). The first studied case exhibited a dryline passage during the simulation window, and the second studied case was used to examine the CBL in a post-cold-frontal environment. The model runs were conducted with three boundary layer parameterization schemes (Yonsei University, Mellor–Yamada–Janjić, and asymmetrical convective) commonly employed within the WRF model environment to represent effects of small-scale turbulent transport. A study domain was centered over the Atmospheric Radiation Measurement Program SGP site in Lamont, Oklahoma. Results show that near-surface flow and turbulence parameters are predicted reasonably well with all tested horizontal grid spacings (1, 2, and 4 km) and that value added through refining grid spacing was minimal at best for conditions considered in this study. In accord with this result, it was suggested that the 16-fold increase in computing overhead associated with changing from 4- to 1-km grid spacing was not justified. Therefore, only differences among schemes at 4-km spacing were presented in detail. WRF model predictions generally overestimated the contribution to turbulence generation by mechanical forcing over buoyancy forcing in both studied CBL cases. Nonlocal parameterization schemes were found to match observational data more closely than did the local scheme, although differences among the predictions with all three schemes were relatively small.

1. Introduction

Atmospheric models utilizing finescale grids with horizontal spacing of 1–4 km are becoming increasingly popular in both research and operational applications. Adequate representation of atmospheric boundary layer flow features within the corresponding horizontal scale ranges poses a certain problem, however. These scales are often within the maximum energy-containing (production) spectral intervals of boundary layer motions. As a result, the corresponding flow features are neither sufficiently resolved explicitly nor correctly represented statistically as subgrid-scale phenomena (Wyngaard 2004). In other words, the inherent assumption of turbulence modeling that an individual model grid cell contains a representative sample of subgrid turbulent motions may not hold within this particular range of scales. This situation brings into question the ability of atmospheric mesoscale models, such as the Weather Research and Forecasting (WRF) model (Skamarock et al. 2008), to accurately reproduce atmospheric flow features on spatial scales of the boundary layer processes—in particular, in terms of near-surface flow, turbulence, and land–atmosphere interaction parameters. Reliable prediction of these fields could prove to be valuable for a wide range of practical applications, including predicting properties of electromagnetic- and sound-wave propagation in the atmospheric surface layer.

In this study, version 3.2.1 of the WRF model was applied to evaluate basic parameters of the atmospheric

Corresponding author address: Jeremy A. Gibbs, School of Meteorology, 120 David L. Boren Blvd., Suite 5900, Norman, OK 73072.
E-mail: gibbz@ou.edu

DOI: 10.1175/2011JAMC2661.1

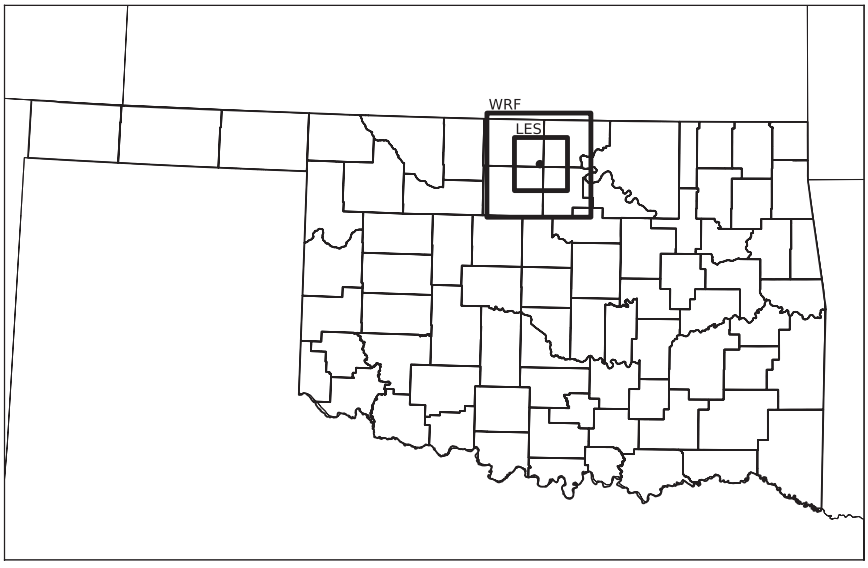

FIG. 1. WRF model domain with 1-km grid spacing (outer square) and LES domain (inner square) centered over the LMN site (indicated with a dot).

turbulent flow for two cases of a dry (also called clear; Holtslag and Duynkerke 1998) atmospheric convective boundary layer (CBL) developing over the southern Great Plains (SGP). In parallel with the WRF model, numerical simulations of the same CBL cases were conducted with the University of Oklahoma large-eddy simulation (LES) code (OU-LES; Fedorovich et al. 2004a,b; Botnick and Fedorovich 2008). Stull (1988) defines the CBL as a mixed layer dominated by buoyant turbulence generation. Over time, the LES approach has proven to be particularly relevant for the reproduction of CBL flow types, whose structure is dominated by large-scale buoyantly produced turbulent eddies (Deardorff 1972; Moeng 1984; Mason 1989; Schmidt and Schumann 1989; Fedorovich et al. 2004b).

The model was run with three different horizontal grid spacings and three different boundary layer/turbulence parameterizations commonly employed in WRF model applications. Both LES and WRF model domains were centered over the SGP observational site of the Atmospheric Radiation Measurement Program (ARM) in Lamont, Oklahoma, (LMN) as shown in Fig. 1. The Lamont site provides for an ideal comparison setting because it offers a robust suite of in situ and remote sensing instrumentation systems. Observational data include atmospheric sounding data available every 6 h, traditional meteorological fields, and surface flux data. The horizontally homogeneous terrain in north-central Oklahoma is mostly suitable for such model and simulation exercises, specifically in relation to the employed version of LES where surface fluxes are prescribed in a horizontally uniform manner.

The investigated CBL cases are described in section 2. Model specifications, setup details, and verification approach are presented in section 3. Model predictions of CBL flow are analyzed in comparison with observational and LES data in section 4. Section 5 contains a summary and conclusions.

2. Studied cases

The CBL cases analyzed in the study were chosen for three main reasons. First, they represent typical daytime summer conditions of the Great Plains. Second, they represent CBL conditions that OU-LES is known to describe adequately. Third, with the goal to address a set of turbulence parameters in full detail, the number of considered cases and model configurations needed to be restricted given space limitations.

a. Dryline (DL) CBL case

The first investigated CBL case was observed from 1200 UTC (0700 local time) 7 June 2007 to 0000 UTC (1900 local time on 7 June) 8 June 2007. This time interval roughly corresponds to the local summer daytime. Few, if any, clouds were present in the CBL over this period of time. The absence of clouds resulted in strong surface heating and was accompanied by moderate to strong winds. As a consequence, a deep sheared CBL developed during the course of the day. These conditions are representative of the CBL type that is known to be confidently reproduced by the OU-LES code (Fedorovich et al. 2004b).

Figure 2 shows the atmospheric soundings at Lamont for 1200, 1800, and 0000 UTC. Initially in the course of

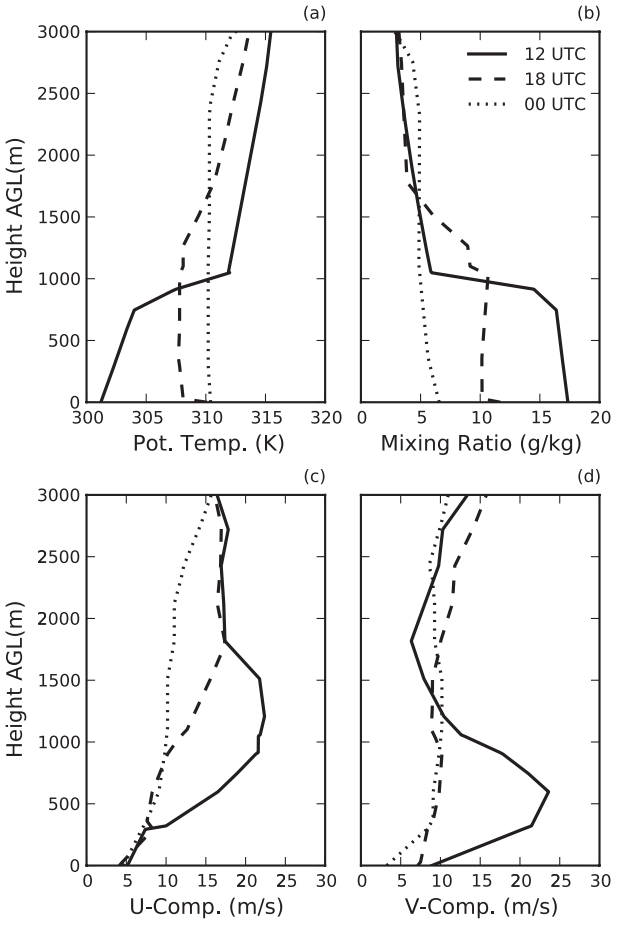

FIG. 2. Atmospheric soundings at the LMN site for 7 Jun 2007 (DL case): (a) potential temperature, (b) water vapor mixing ratio, (c) u component of wind, and (d) v component of wind. Solid, dashed, and dotted lines correspond, respectively, to 1200, 1800, and 0000 (following day) UTC.

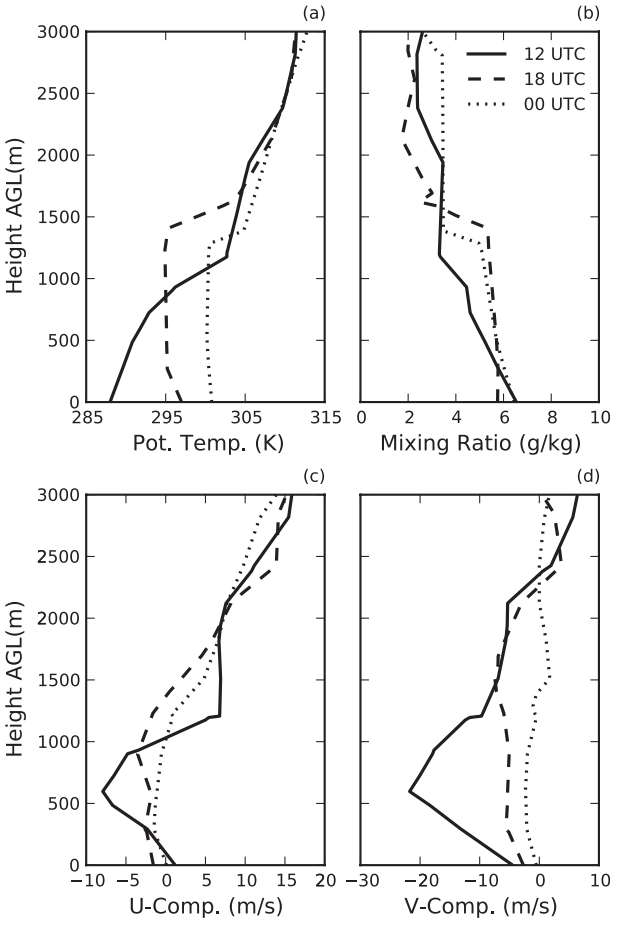

FIG. 3. As in Fig. 2, but for 8 Jun 2007 (CF case).

CBL development, a strong southwest low-level jet (LLJ) was present, with the potential temperature profile indicating a stably stratified layer near the surface. The near-surface humidity was relatively high. To the west of the Lamont site, a dryline formed and began to propagate eastward. By midmorning into early afternoon, the dryline passed through the site, which resulted in the associated decrease in low-level moisture. Within the CBL, wind speed and shear also decreased. This CBL case is particularly interesting because it allows one to evaluate the ability of the WRF model to reproduce a highly temporally heterogeneous environment in which the combined shear and buoyancy forcing drive CBL growth.

b. Cold-frontal (CF) CBL case

The second modeled CBL case was observed from 1200 UTC (0700 local time) 8 June 2007 to 0000 UTC (1900 local time on 8 June) 9 June 2007. As in the DL case, conditions present on this day are well within the operational range of the OU-LES code. Figure 3 shows the atmospheric soundings at the Lamont site for 1200, 1800, and 0000 UTC. Between 0300 and 0600 UTC 8 June 2007, a cold front passed through the site, bringing associated lower temperatures. In the initial portion of the simulation time window, a north-northwest LLJ was present and the surface potential temperature was approximately 15 K lower than at the same time during the previous day. To the northwest, a high pressure system was building in the southeast direction. By midday, the high pressure system moved closer to the Lamont site, resulting in decreased wind speeds. Toward the end of the simulation window, the high pressure system was centered directly over the Lamont site and the wind speeds at the site nearly died off entirely.

In comparison with the DL case, this case was characterized by lower temperatures, weaker winds, and relatively constant humidity throughout the CBL. A decrease in sensible heat flux resulted in decreased buoyancy flux and, as a consequence, a shallower CBL. Because shear

effects were diminished as a result of weaker winds, CBL growth was primarily due to the buoyancy forcing. This case tests the ability of the WRF model to reproduce meteorological conditions in a post-cold-frontal environment in which development of the CBL is mainly controlled by the buoyancy driving mechanism.

3. Experimental design

a. Simulation and model setup

1) OU-LES

Large-eddy simulations were run in a numerical domain of $51.1 \times 51.1 \times 4\ \text{km}^3$ centered over the Lamont site, with horizontal spacing $\Delta x = \Delta y = 100$ m and vertical spacing $\Delta z = 50$ m. The first model level was located at 25 m AGL. The OU-LES code employs a subgrid turbulence kinetic energy closure that is modeled after that in Deardorff (1980). Surface fluxes in the simulations were prescribed from the eddy correlation flux measurement system (ECOR; Cook and Pekour 2008) at the Lamont site, with flux values being available in 30-min intervals. To account for the larger-scale (as compared with the size of the LES domain) atmospheric variability, a force–restore nudging procedure was implemented in the OU-LES. The solutions for horizontal velocity components, virtual potential temperature, and water vapor mixing ratio at each time step were nudged with temporally interpolated profiles (soundings) from the Rapid Update Cycle (RUC; Benjamin et al. 1994) model. The following force–restore (f–r) term was incorporated in the filtered LES equations:

$$\left(\frac{\partial \tilde{\phi}}{\partial t}\right)_{\text{f-r}} = -\frac{\overline{\tilde{\phi}}(z)_{\text{LES}} - \phi(z)_{\text{RUC}}}{t_r},$$

where $\tilde{\phi}$ is the considered resolved (i.e., filtered in the LES sense) flow variable, $(\partial\tilde{\phi}/\partial t)_{\text{f-r}}$ is its tendency due to the nudging (force–restore mechanism), $\overline{\tilde{\phi}}(z)_{\text{LES}}$ is the mean (obtained by averaging over horizontal planes) profile of $\tilde{\phi}$ from the preceding time step, $\phi(z)_{\text{RUC}}$ is the RUC profile of the flow variable at that time step, and t_r is the nudging time constant, which was set equal to 3600 s. Hence, the tendencies of the above-specified physical variables are adjusted across the entire domain every time step by subtracting the time-scaled difference between the domain-averaged profiles from OU-LES and the local profile from RUC at the previous time step. The time constant regulates the rate of adjustment of the spatially averaged LES fields to the RUC profiles that represent the larger-scale atmospheric fields.

2) WRF MODEL

The WRF model was run in three domains (all being centered at the Lamont site), with horizontal grid spacings of 1, 2, and 4 km. All three domains had the same 101×101 horizontal grid with 41 vertical levels. The first model level was located at 8 m AGL. All initial and lateral boundary conditions were provided from North American Regional Reanalysis (Mesinger et al. 2004) data. A 12-h warm start was used to allow for model spinup. Model settings for microphysics, longwave radiation, shortwave radiation, land surface model, and horizontal diffusion closure were held the same for all model runs. The corresponding parameterizations were, respectively, the WRF Single-Moment 6-Class Scheme (Hong et al. 2004), Rapid Radiative Transfer Model (Mlawer et al. 1997), fifth-generation Pennsylvania State University–National Center for Atmospheric Research Mesoscale Model (MM5) shortwave-radiation scheme (Dudhia 1989), Noah Land Surface Model (LSM; Chen and Dudhia 2001), and the horizontal deformation first-order closure scheme (Smagorinsky 1963). The surface layer (SL) and planetary boundary layer (PBL) schemes of the WRF model were varied in conjunction with horizontal grid spacing.

The employed SL/PBL scheme combinations were MM5 (Paulson 1970)/Yonsei University (YSU; Hong et al. 2006), Eta (Janjić 1996, 2001)/Mellor–Yamada–Janjić (MYJ; Janjić 1990, 1996, 2001), and Pleim–Xiu (PX; Pleim 2006)/Asymmetrical Convective Model, version 2 (ACM; Pleim 2007), with each pair being applied with 1-, 2-, and 4-km grid spacings. Note that the version of the ACM introduced in Pleim (2007) is called the ACM2 in that reference to indicate that the scheme is the second version. In our study, this second version of the ACM scheme is denoted simply as ACM (without the "2"). This is done to avoid confusion with the name of a WRF model run (see section 4) in which the ACM scheme is employed with 2-km grid spacing, for which reason the run is titled ACM2. Brief descriptions of each scheme are given below. For further information regarding the employed SL/PBL schemes, see the WRF model technical description (Skamarock et al. 2008) and references therein.

The YSU scheme utilizes nonlocal diffusion in the mixed layer and local diffusion in the free atmosphere. For the mixed-layer ($z \leq h$), where h is the boundary layer depth, the turbulent diffusion equation for any prognostic variable a is given by

$$\frac{\partial a}{\partial t} = \frac{\partial}{\partial z}\left[K_a\left(\frac{\partial a}{\partial z} - \gamma_a\right) - \overline{(w'a')}_h\left(\frac{z}{h}\right)^3\right],$$

where K_a is the corresponding eddy diffusivity; γ_a is the countergradient correction term, which incorporates the contribution of the large-scale eddies to the total flux; and $\overline{(w'a')}_h$ is the flux at the inversion layer. The YSU scheme

explicitly treats the entrainment process through the asymptotic flux term at the inversion layer, $\overline{(w'a')}_h(z/H)^3$. Within the entrainment zone, the total diffusivity is found by taking the geometric mean of the entrainment diffusivity and the local diffusivity. In the free atmosphere, the YSU scheme utilizes a local diffusion scheme, or the so-called local-K approach.

The MYJ scheme (Janjić 2001) implements a nonsingular version of the Mellor and Yamada (1982) level-2.5 closure scheme. The prognostic turbulence kinetic energy (TKE) equation in the Mellor and Yamada (1982) scheme is parameterized as

$$l\frac{d\left(\frac{1}{q}\right)}{dt} = \frac{\alpha\left(\frac{l}{q}\right)^4 + \beta\left(\frac{l}{q}\right)^2}{\gamma\left(\frac{l}{q}\right)^4 + \delta\left(\frac{l}{q}\right)^2 + 1} - \frac{1}{B_1},$$

where l is the master length scale, q is the square root of twice the TKE, and B_1 is a constant. The coefficients denoted by Greek letters only depend on buoyancy and shear of large-scale flow. The length scale is first determined from diagnostic equations and is then adjusted to satisfy a nonsingularity criterion as described in Janjić (2001). The diffusion coefficients are computed from q and l.

The ACM scheme (Pleim 2007) offers a revised version of the original asymmetrical convective model (ACM1) described in Pleim and Chang (1992). The ACM1 scheme evaluated nonlocal fluxes through a transilient matrix, which controlled the mass flux between any two model layers. As noted in Pleim (2007), the main drawback of ACM1 was the lack of local upward diffusion, which resulted in an unrealistic step function between the first two model layers. To correct this problem, an eddy diffusion component of nonlocal transport was added in the current version of the ACM scheme. The essential parameter dictating the proportion of local versus nonlocal mixing in the ACM scheme is f_{conv}. For stable or neutral conditions, $f_{\text{conv}} = 0$ and the ACM scheme defaults to pure eddy diffusion. Once the breadth of convective eddies exceed that of the vertical grid spacing, f_{conv} is allowed to vary from 0 to 1. Pleim (2007) derives an expression for f_{conv} through the ratio of nonlocal flux to the total flux. Results indicated that, as flow features evolve from stable and neutral regimes to convective conditions, f_{conv} levels off at a value of 0.5.

The physical schemes that are held the same in our experiments with different SL/PBL parameterizations represent a sensible set of physical scheme options in the WRF model. In combination, these schemes serve as a baseline environment to test sensitivity of turbulent flow predictions by the WRF model to SL/PBL schemes in conjunction with varying horizontal grid spacing. One might claim that certain baseline schemes work better than others, but it is beyond the purview of this study to evaluate these schemes. It is more important to hold them unchanged so that the WRF model sensitivity to the choice of an SL/PBL scheme combination may be discerned. There are model studies in which model physics have been arbitrarily changed between configurations yet still attempt to ascertain model solution dependence on specific SL/PBL parameterizations. In our opinion, it is crucial to single out the tested schemes as much as possible to avoid added ambiguities in interpreting the model predictions.

b. Verification approach

In modeling studies, the matter of validating model results with data that represent the actual atmospheric state is a recurrent issue. One inherent problem of such a comparison is that model data for one grid cell represent the local atmospheric state as a statistical mean over the cell while observational data are usually collected at a single location arbitrarily positioned with respect to the model grid. In this sense, to compare single-point observations with model results is problematic. As is the case in our study, however, if the area over which the comparison is undertaken is (or may be considered to be) homogeneous in a statistical sense, then the comparison of atmospheric boundary layer flow statistics obtained with different schemes and with different grid spacing appears to be sensible.

To facilitate the outlined comparison, the WRF model data were extracted for the subset of cells that coincided with the OU-LES domain. In that sense, the OU-LES grid acted as the comparison domain. Within this comparison domain, horizontal averages were taken of both WRF and OU-LES data for each respective output time to produce mean vertical profiles over the Lamont site. This proves to be a reasonable approach since the land surface properties in north-central Oklahoma are fairly homogeneous. For potential temperature and water vapor mixing ratio, both the WRF model and OU-LES data were extrapolated to 2 m AGL by following Monin–Obukhov similarity theory (Monin and Obukhov 1954; Dyer and Hicks 1970). This level coincided with the measurement height of the ARM surface meteorological observation system (SMOS; Ritsche 2008). For wind speed and direction, both WRF model and OU-LES data were similarly extrapolated to the SMOS observation level of 10 m AGL. The extrapolated values were then additionally averaged in time to produce hourly means. This averaging allowed for removal of small-scale temporal perturbations and numerical noise. The resultant data were used to compare parameters of the near-surface atmospheric structure over time periods that

carried both mesoscale and synoptic-scale signals. For turbulence fields, WRF model and OU-LES data were compared with both ECOR and the ARM carbon dioxide flux measurement system (CO2FLX; Fischer 2005). Although the Lamont site measurements represent single points in space, their inclusion provides a real-world component for model validation. The observational data are not meant to provide an exact statistical verification but rather to offer a relative gauge of how the WRF model represents near-surface atmospheric structure and its evolution. Such evaluation of model behavior is of particular interest for our study.

c. *Evaluated turbulence and boundary layer parameters*

Evaluated parameters of the near-surface turbulence regime were represented by near-surface values of vertical turbulent fluxes of heat, both sensible, $\rho c_p \overline{w'\theta'}$, and latent, $\rho L_v \overline{w'q'}$, and components of the vertical turbulent kinematic momentum flux, $\overline{w'u'}$ and $\overline{w'v'}$. In these expressions for fluxes, which are assumed to be approximately height constant within the surface layer, w is the vertical velocity component, u and v are the horizontal velocity components, θ is the potential temperature, q is the specific humidity of the air, ρ is the air density, L_v is the latent heat of vaporization for water, the overbars denote Reynolds averaging, and the primes denote turbulent fluctuations with respect to corresponding mean (Reynolds averaged) flow variables. The indicated turbulence parameters were used to evaluate the following three characteristics of the near-surface turbulence regime: the friction velocity, given by

$$u_* = [(\overline{w'u'})^2 + (\overline{w'v'})^2]^{1/4}$$

and commonly employed as a boundary layer turbulence velocity scale (Stull 1988), the turbulence temperature scale

$$\theta_* = -\overline{w'\theta'}/u_*,$$

and the vertical turbulence buoyancy flux

$$B = \frac{g}{\theta_0}\overline{w'\theta'_v} = \frac{g}{\theta_0}\overline{w'\theta'} + 0.61g\overline{w'q'},$$

where g is the acceleration due to gravity, θ_v is the virtual potential temperature (approximated as $\theta_v = \theta + 0.61\theta_0 q$), and θ_0 is a constant temperature reference value.

Depth of modeled/simulated CBL was evaluated from the domain-averaged (mean) virtual potential temperature profile. The position of the CBL top z_i was estimated from the elevation of the maximum gradient of the mean θ_v profile (gradient method) in the upper portion of the CBL as described in Fedorovich et al. (2004a,b). The negative ratio of z_i to the Obukhov length $[L = -u_*^3/(\kappa B)]$, given by

$$-\frac{z_i}{L} = \kappa\frac{w_*^3}{u_*^3},$$

where κ is von Kármán's constant (adopted to be 0.4) and $w_* = (Bz_i)^{1/3}$ is the convective velocity scale originally suggested by Deardorff (1970), provides the CBL integral stability parameter. In the CBL, u_*^3 and w_*^3 may be regarded as measures of the TKE production by surface wind shear and surface buoyancy, respectively (Stull 1988). Thus, the stability parameter $-z_i/L$ conveniently characterizes relative roles of buoyant and shear forcings in driving the sheared CBL. The Obukhov length scale is negative in the CBL (where $B > 0$), and therefore $-z_i/L$ is positive.

Because each of the considered boundary layer schemes in the WRF model utilizes its own respective algorithm to determine the BL depth (whose corresponding value is revealed in the WRF model output file), a unified procedure consistent with evaluation of the CBL depth by the gradient method described above was implemented to retrieve z_i from the domain-averaged (mean) virtual potential temperature field predicted by the WRF model. The gradient method was also used to estimate z_i from Lamont observational data.

4. Results

a. *Grid-spacing effects*

Given the current trend of decreasing horizontal grid spacing in mesometeorological atmospheric models, it is important to assess whether there is an inherent benefit from refining the grid spacing from 4 to 1 km that outweighs the increased computational burden. In this study, there were only a few fields in which discernible differences between predictions with disparately spaced grids were found. Although one might expect unequivocal improvement as grid spacing is reduced, results indicated inconsistent behavior in this regard. For instance, in the DL case potential temperature and horizontal wind speed degraded in comparison with observations when the grid spacing was refined, whereas in the CF case the same was true for friction velocity (turbulence velocity scale) and the stability parameter. For other considered fields, such as turbulence temperature scale and near-surface sensible ($\rho c_p \overline{w'\theta'}$) and latent ($\rho L_v \overline{w'q'}$) heat fluxes, differences in the same scheme at different grid spacing did exist but were not appreciable. These findings

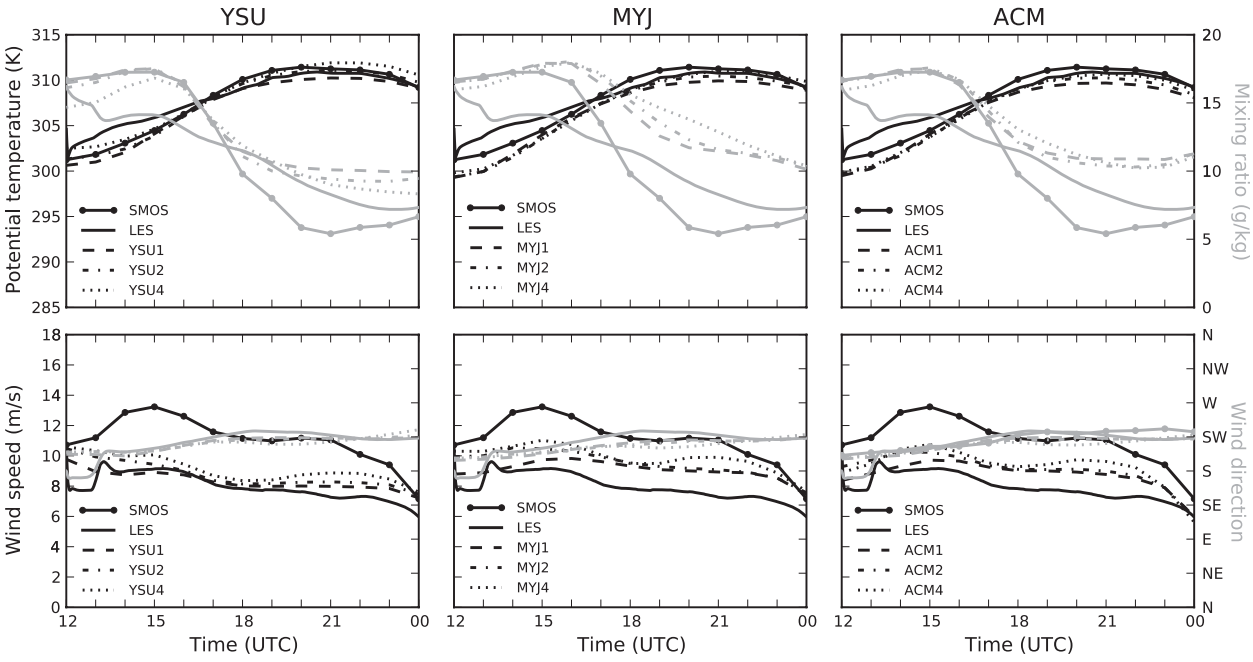

FIG. 4. Evolution of (top) potential temperature (black lines) and water vapor mixing ratio (gray lines) and (bottom) wind speed (black lines) and wind direction(gray lines) predicted by the WRF model with (left to right) different parameterization schemes and different grid spacings (denoted by the number after the scheme label in the keys) for 7 Jun 2007 (DL case). Observational (SMOS) and LES data are also shown for comparison.

resemble those from Kain et al. (2008) and Schwartz et al. (2009) in which it was shown that reducing horizontal grid spacing in operational models from a spacing of 4 km to a spacing of 2 km offered little, if any, increased value in forecast guidance. Although those studies focused on convection and precipitation forecasts, the same reasoning applies since theoretical assumptions in the respective parameterizations become less justifiable within these particular scale ranges.

1) DL CASE

Figure 4 illustrates the effects of changing grid spacing for potential temperature, water vapor mixing ratio, wind speed, and wind direction. While keeping in mind that WRF model values at 1200 UTC represent a 12-h forecast because of the warm-start procedure, it is seen that potential temperature and water vapor mixing ratio values were smaller than observational values for all schemes. As the day progressed, WRF model predictions for potential temperature continued to show smaller values than observations while predicted water vapor mixing ratio values were too small prior to the dryline passage and too large after the passage. For both the potential temperature and mixing ratio, WRF model time evolution matched the physical trend better than did OU-LES, which was unable to reproduce relatively sharp changes in the meteorological fields associated with dryline motion. This inability of OU-LES to treat boundary layer flows with sharp gradients of meteorological fields along the simulation domain has been marked out in Conzemius and Fedorovich (2008). Differences among model outputs with different grid spacing values were small for each scheme, with model runs using 4-km spacing often comparing more favorably to observations for potential temperature. Modeled horizontal wind speed values were systematically underpredicted with all turbulence-scheme and grid-spacing combinations. When differences between outputs with different grid-spacing values were notable, model configurations employing 4-km spacing reproduced values closer to observations. Wind direction estimates were nearly identical to observations and OU-LES data for all scheme/spacing combinations, with inconsequential differences related to grid-spacing variations.

Comparison of model flux predictions with Lamont observations yielded striking discrepancies. Because the OU-LES was driven with surface fluxes observed at the Lamont site, it would be redundant to include here for comparison surface flux values from LES. Surface sensible heat flux values predicted by the WRF model were systematically and significantly lower when compared with the observed values, and surface latent heat flux values were grossly overestimated. Differences between model predictions with different grid spacings were small

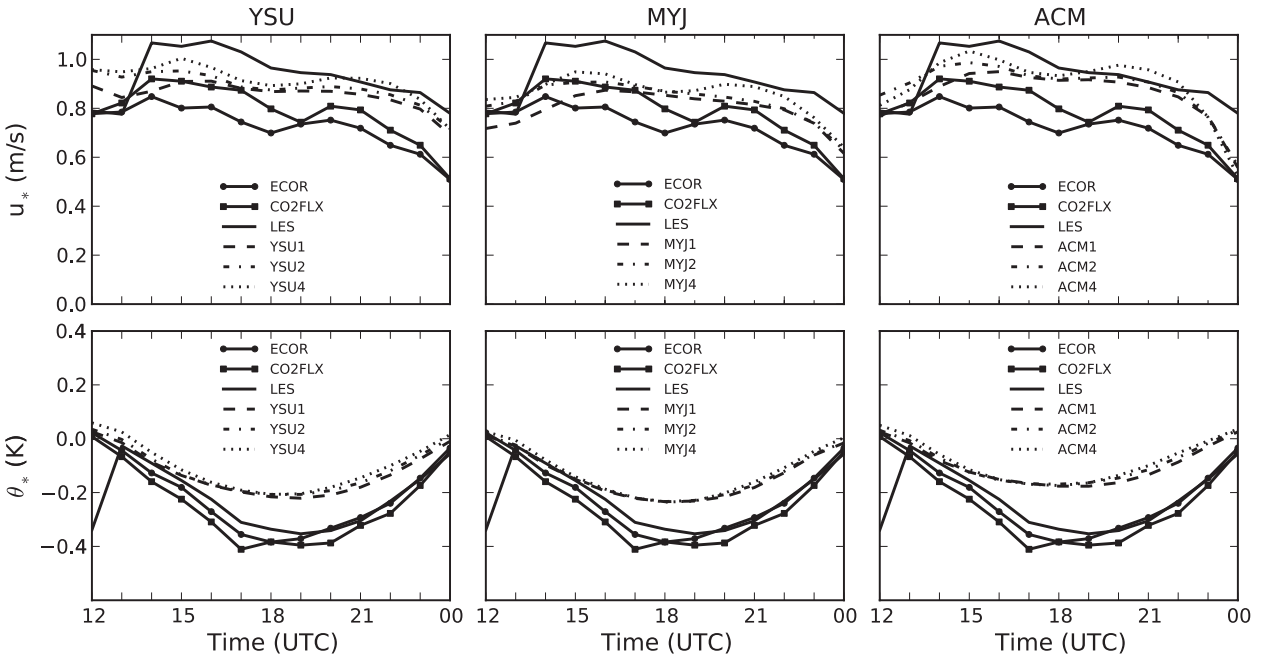

FIG. 5. Evolution of (top) friction velocity u_* and (bottom) temperature scale θ_* predicted by the WRF model with (left to right) different parameterization schemes and different grid spacings (denoted by the number after the scheme label in the keys) for 7 Jun 2007 (DL case). Observational (ECOR and CO2FLX) and LES data are also shown for comparison.

and inconsequential, however, and hence the corresponding data are not shown. The noted large discrepancies in sensible and latent flux values are discussed in section 4b.

WRF model predictions of turbulence velocity scale and turbulence temperature scale are of importance for many practical applications that employ near-surface turbulence parameters, for example, for evaluating the properties of electromagnetic- and sound-wave propagation in the atmospheric surface layer. Figure 5 illustrates the effects of changing grid spacing on turbulence parameters among the three investigated WRF PBL schemes. Time evolution of u_* predictions from all nine WRF model configurations closely matches phase with observations and is closer to observed values than is OU-LES. Each configuration produces a systematic overprediction, however. The behavior of θ_* predictions matches the phase of the time trace of observations. All employed combinations of SL/PBL schemes and grid spacings systematically underpredict θ_* as compared with both OU-LES and Lamont data, and differences among schemes are consistently small. In general, refined grid spacing in this particular case led to slightly more realistic model predictions of both u_* and θ_*.

Values for PBL depth estimates were smaller for all WRF model configurations early in the simulation window as compared with both OU-LES and observational data. As the CBL developed, the PBL depth estimates from the WRF model became largely overpredicted. In all cases, reducing the grid spacing led to more-realistic depth estimates. Except for the beginning and ending periods of the simulation window, all WRF model predictions of the stability parameter matched closely with both OU-LES and observational data. Given the previously discussed behavior of u_*, such discrepancies should be expected. Differences between WRF model predictions with different grid spacing were inconsequential during portions of the day with peak convective activity (the corresponding data are not shown).

2) CF CASE

Figure 6 illustrates the effects of changing grid spacing on potential temperature, water vapor mixing ratio, wind speed, and wind direction. As a result of the cold-frontal passage, temperature values in this CBL case were predictably lower than in the DL counterpart. Changes in grid spacing resulted in minimal differences in relation to the observational data, and the time evolution was also reproduced very accurately. Modeled horizontal wind speeds mirrored observational values, and OU-LES values were larger than observed, especially over the first half of the day. In this case, sensitivity to grid spacing in the WRF model predictions degraded with grid refinement. With the coarser grid, the WRF model had trouble with the placement of the impinging high pressure system, as is evident from wind direction predictions. A noticeable improvement in this respect

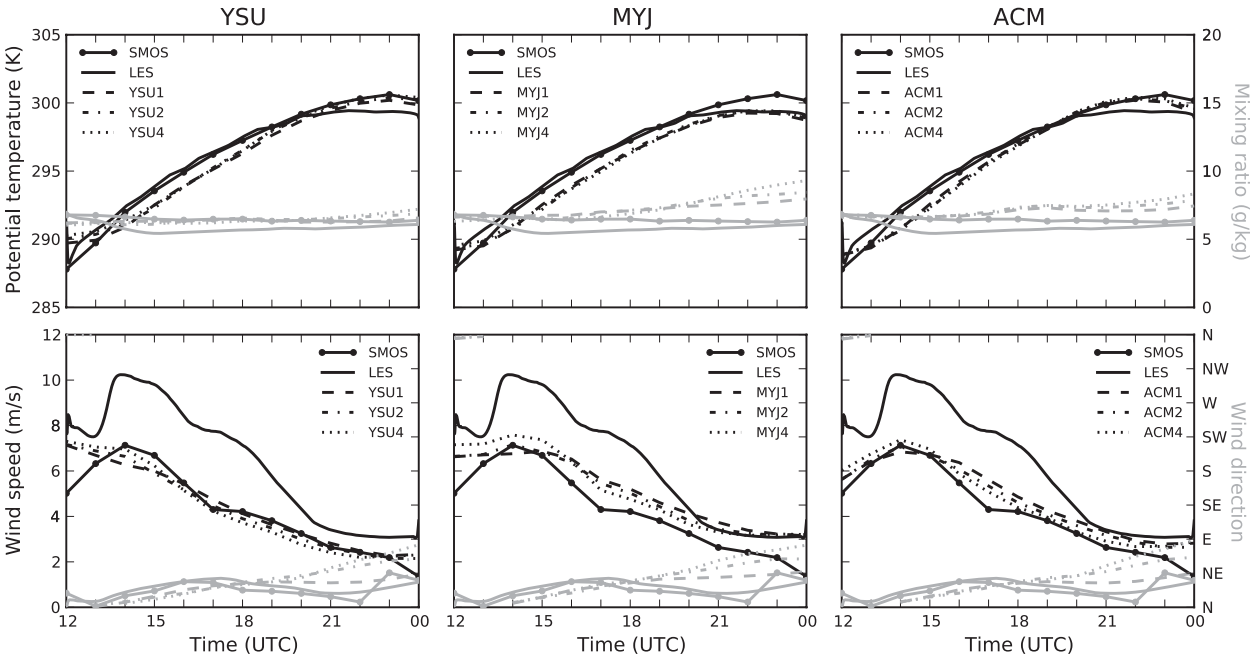

FIG. 6. As in Fig. 4, but for 8 Jun 2007 (CF case).

occurred when moving from a 4-km mesh to a 1-km mesh.

In the CF case, surface sensible heat flux fields from the WRF model matched observations closely, both in magnitude and evolution. Meanwhile, the surface latent heat flux was again overpredicted with all employed combinations of model settings, although by a far smaller amount than in the DL case. The flux values were generally insensitive to changing grid spacing. Again, given the uniformity of terrain properties within the comparison domain, this consistency is expected.

Figure 7 illustrates the effects of grid spacing on turbulence velocity scale and turbulence temperature scale. Friction velocity u_* is again, as in the DL case, overpredicted with all three PBL schemes and three grid spacings employed. On several occasions during the day, the predicted values of u_* are up to 2 times the observed values. Differences between WRF model predictions with different grid spacing were small, with those employing 4-km spacing often performing more favorably as compared with observations. Such discrepancies are small, however. The turbulence temperature scale predicted by the WRF model matches closely OU-LES data but was once again underpredicted when compared with observational data. Sensitivity to grid spacing for this parameter is negligibly weak.

Across all configurations of the WRF model, estimates of PBL depth matched closely with OU-LES data and were underpredicted as compared with observations. In this particular case, the WRF model appears to be insensitive to grid spacing variations between 1 and 4 km. As in the DL case, WRF model predictions for the stability parameter agreed closely the OU-LES data. The predictions were notably smaller than the observations, however. Once again, the sensitivity to u_* is evident when considering this discrepancy. Grid-spacing effects were negligible for the stability parameter in this case.

b. Boundary layer scheme effects

Differences in model predictions of flow parameters using different SL/PBL turbulence schemes were found in the investigated cases to be generally larger than the differences associated with varied grid spacing in the WRF model. Since grid spacing effects were overall minor (see the previous section), results of varying SL/PBL parameterizations will only be presented for WRF model configurations with the 4-km grid spacing. We focus on this particular grid spacing because, in our opinion, the previously discussed resolution sensitivities do not warrant the required 16-fold increase in computational grid size to cover the same geographical domain for a WRF model run under conditions considered in this study.

1) DL CASE

Figure 8 illustrates a meteogram (timeline trace) of basic meteorological variables derived from WRF model output, OU-LES data, and measurements at the Lamont site. Remembering that the 1200 UTC values from the

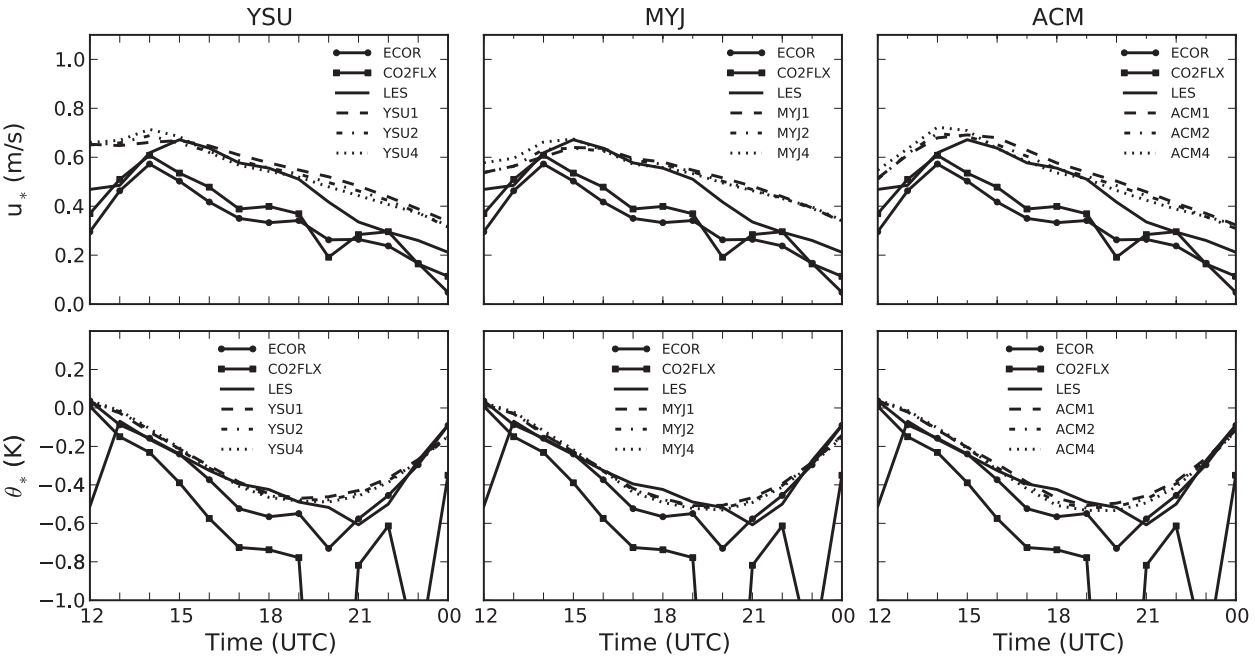

FIG. 7. As in Fig. 5, but for 8 Jun 2007 (CF case).

WRF model represent conditions achieved after a 12-h spinup whereas OU-LES is initialized with local 1200 UTC profiles retrieved from the RUC data, one immediately notes a common problem for employed SL/PBL schemes in the WRF model at the beginning of the day: except for the YSU scheme, they all predict cooler and drier atmospheric conditions as compared with the observed temperature and water vapor mixing ratio. With both the YSU and ACM schemes, the WRF model confidently reproduces the sharp decrease in moisture associated with the dryline passage, whereas the MYJ scheme fails to capture the evolution pattern. The OU-LES also predicts much more gradual changes in the mixing ratio than the observations show. In both cases, however, the magnitude of the moisture drop is not well reproduced. Wind speed and direction predictions with different schemes are close to each other, with the MYJ and ACM schemes producing results that are slightly closer to observations than does the YSU scheme. Wind speeds from the WRF model are closer to observational data than are those from OU-LES. Although the speed values are underpredicted, they closely match the semidiurnal pattern of the wind.

Drastic differences between WRF model predictions and observational heat flux data for the DL case are evident in Fig. 9 (left-hand side). The surface sensible heat flux is hugely underpredicted, and the surface latent heat flux is grossly overpredicted. One can look at the total heat flux (sensible flux added to latent flux) and compare it with the total heat flux distribution in the CF case shown in the same figure. In both studied cases, the evolution patterns of the total flux are consistent with each other and with anticipated variations of the surface buoyancy flux in the clear CBL at the Lamont site. This result points to an apparent problem with heat flux partitioning in the modeled DL-case CBL. The exact cause of this problem is not clear, but it is possibly a culprit of the Noah land surface scheme (Chen and Dudhia 2001) employed in the WRF model and coupled with the SL/PBL scheme. In addition, the disparity between two instruments, ECOR and CO2FLX, at the same location illustrates that instrumentation error is also possible. For both heat fluxes, model predictions with YSU and MYJ schemes are slightly closer to observations than are those with the ACM scheme.

The noted discrepancies in flux partitioning are disconcerting. Among the physics schemes that are held constant in our WRF model runs, one can easily argue that the LSM is most closely tied to the SL/PBL schemes. In accord with this argument, all studied cases were rerun using the PX LSM (Pleim and Xiu 1995; Xiu and Pleim 2001) in place of the Noah LSM with the hope of resolving the partitioning issue. Results from these simulations are not shown here for sake of brevity. The PX LSM produces a smaller latent heat flux that is closer to the observational data from the LMN site. The corresponding values of the sensible heat flux are slightly larger and closer to observations than are values obtained

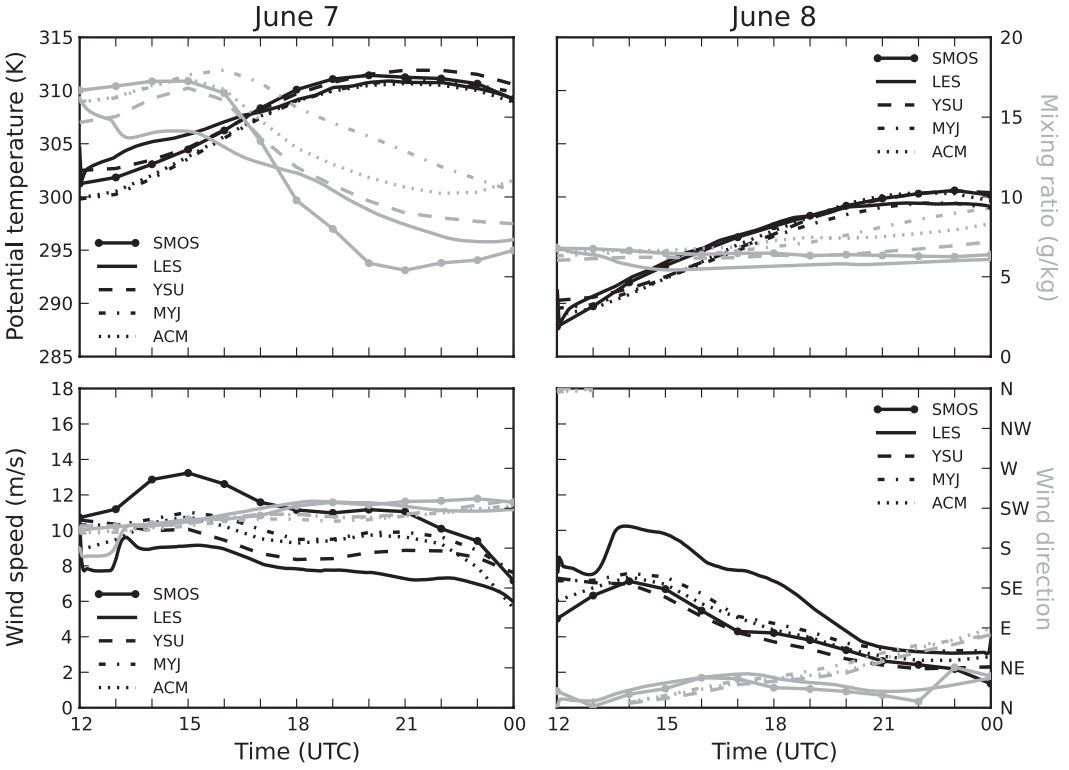

FIG. 8. Evolution of (top) potential temperature (black lines) and water vapor mixing ratio (gray lines) and (bottom) wind speed (black lines) and wind direction (gray lines) predicted by the WRF model with different parameterization schemes for (left) 7 Jun 2007 (DL case) and (right) 8 Jun 2007 (CF case). Observational (SMOS) and LES data are also shown for comparison.

with the Noah LSM, although the change is somewhat modest. This seems to be a desirable tendency. Closer inspection of produced soil moisture values tempered this finding, however. The Noah LSM appears to better reproduce soil moisture than does the PX LSM. This means that, departing farther from observations, soil moisture produced with the PX scheme artificially improves the latent flux values, with the flux-partitioning error still being in place. These findings present an example of what a typical user may encounter while modeling meteorological conditions considered in this case. In an applied framework, the unnatural correction of the model to account for this error is simply not practical or physically coherent.

Turbulence scales for velocity and temperature are shown on Fig. 10. Both OU-LES and the WRF model produce u_* values that are larger than the observed ones, thus overpredicting the mechanical turbulence generation. The MYJ scheme predicts values that are slightly closer to observations than are those of the YSU and ACM schemes, although results with all three schemes follow the same evolution pattern. The magnitude of the turbulence temperature scale is underestimated by all three SL/PBL schemes in the WRF model as compared with OU-LES values that agree with the Lamont observational data decently. Such behavior of the modeled θ_* is expected given the WRF-model overprediction of friction velocity and the underprediction of surface sensible heat fluxes. Differences among predictions with different SL/PBL schemes are minor, with the ACM scheme producing results that are farthest from observations.

When inspecting Fig. 11, it may appear on the surface that the SL/PBL schemes in the WRF model produce too sharp of an increase of the CBL depth, but, given that there are only two available data points from the Lamont site that provide estimates of the CBL depth and taking into account the previously noted OU-LES failure to capture the sharp changes in meteorological fields associated with the dryline passage, it is entirely possible that the WRF model more accurately represents the CBL depth evolution than OU-LES does. Differences among predictions from the YSU and ACM schemes are small, and the MYJ scheme produces the shallowest CBL early into the day and predicts the sharpest increase in CBL depth during the dryline passage. Such performance of the MYJ scheme is apparently

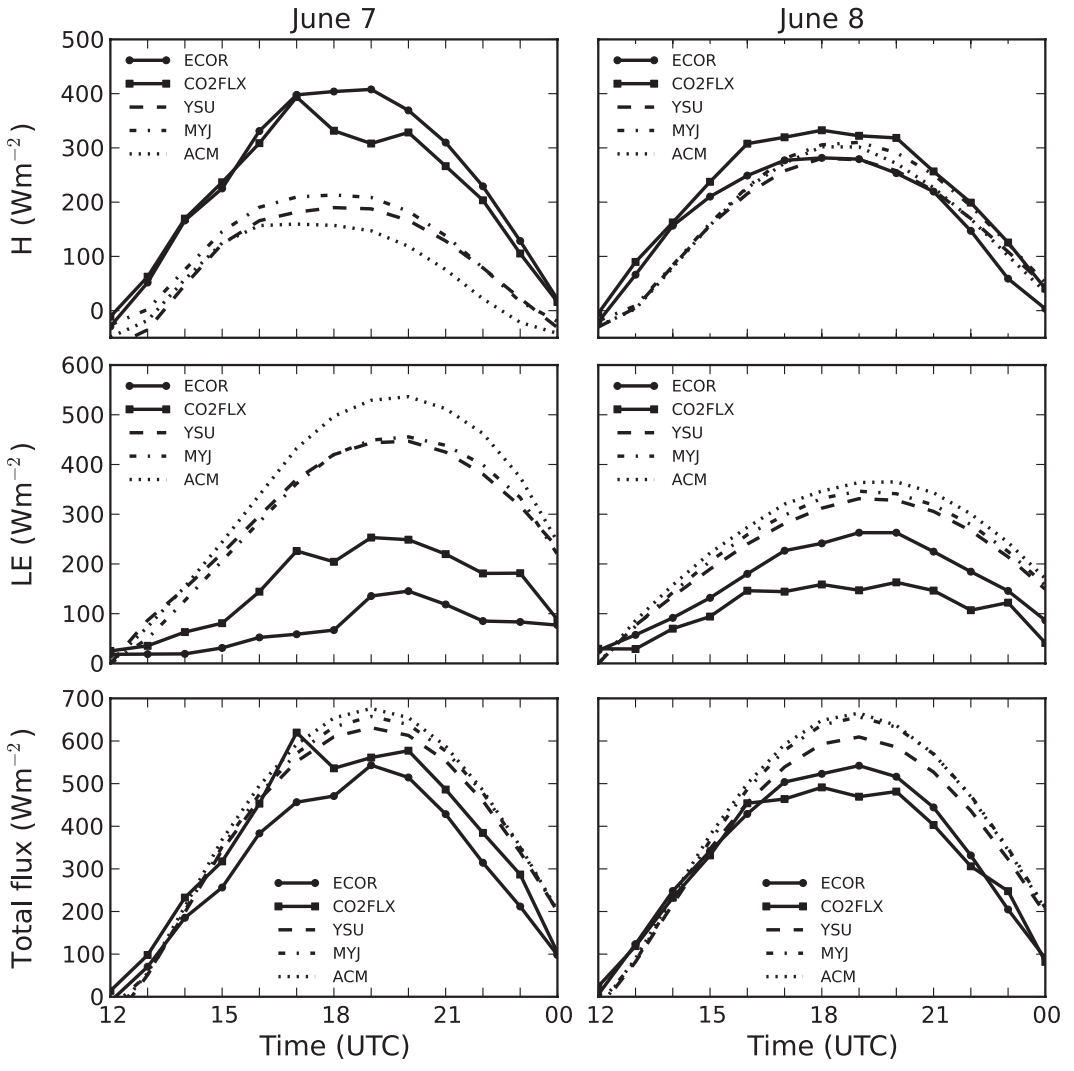

FIG. 9. Evolution of the near-surface (top) sensible, (middle) latent, and (bottom) total heat fluxes predicted by the WRF model with different parameterization schemes for (left) 7 Jun 2007 (DL case) and (right) 8 Jun 2007 (CF case). Observational data (ECOR and CO2FLX) are also shown for comparison.

associated with its local nature, which results in weaker and slower mixing throughout the evolving CBL. In terms of the stability parameter $-z_i/L$, all tested SL/PBL schemes produce values that are close to the OU-LES results for times of peak convective activity, although all numerical methods predict stronger shear contribution to the CBL turbulence regime than the observations indicate. This feature is primarily caused by the overproduction of near-surface turbulence by shear in the WRF model and OU-LES.

2) CF CASE

Figure 8 (right panels) illustrates the meteogram for the CF-case CBL. The smaller initial values that were previously observed in the WRF model predictions for the DL case are not as prevalent in the predicted potential temperature and humidity evolution patterns. Differences among predictions using different schemes are minimal for potential temperature, with the YSU and ACM schemes being closer to observations while the MYJ scheme again reproduces humidity values that differ most from observations. OU-LES values for wind speed are considerably overpredicted, whereas WRF model predictions are only slightly larger than observed values of the wind speed. The YSU scheme nearly matches the observational trace perfectly in this regard, with predictions using MYJ and ACM schemes being close to each other. This slight model overprediction of wind is most noticeable early in the day. Differences between the WRF model predictions with different schemes

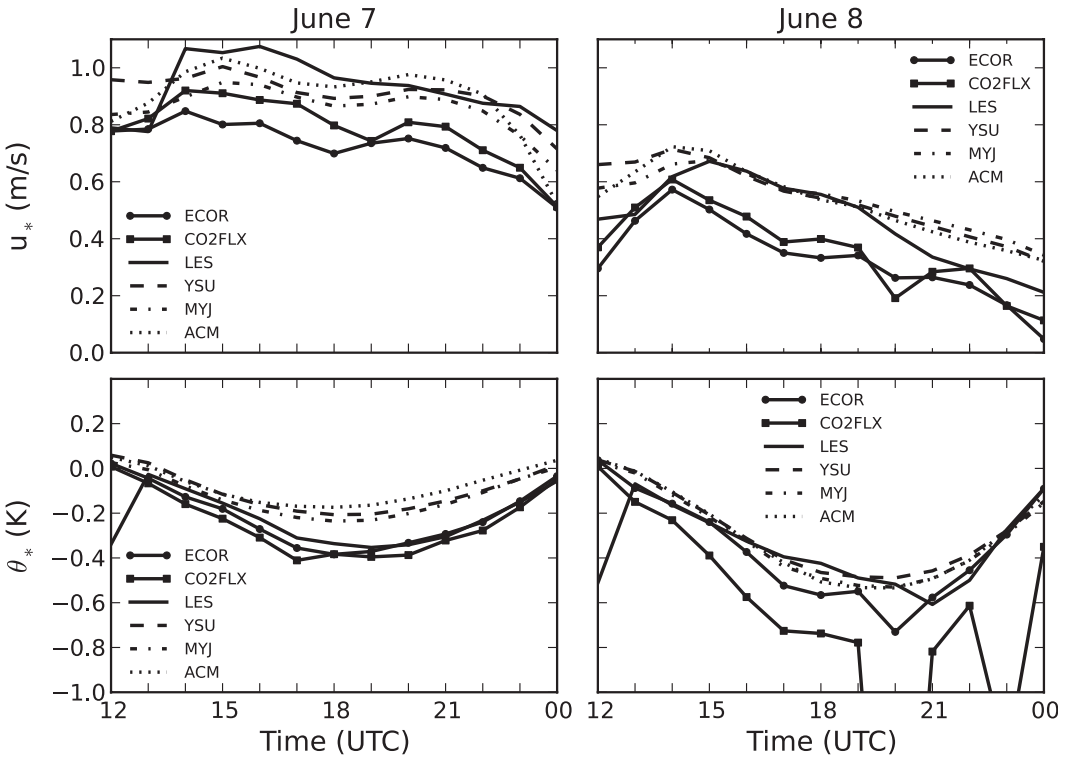

FIG. 10. As in Fig. 9, but for (top) u_* and (bottom) θ_*.

are negligible for wind direction for the first half of the day, with values diverging substantially in the second half of the simulation window. This indicates a phase error in the large-scale high pressure system placement in the WRF model.

The predicted evolution patterns of the turbulent heat flux components in this case look much more reasonable than in the DL case, as seen in Fig. 9. Differences among predictions with different schemes are very small for the near-surface sensible heat flux, and the time evolution of the flux and its magnitude values match observations closely. With all three schemes, the WRF model still overestimates the latent heat flux, although not as drastically as in the DL case. Predictions using the YSU scheme are closest to the observed values, whereas the ACM scheme results in the largest deviations from the measured values. The total flux distribution looks nearly identical to its counterpart in the DL case, leading credence to the flux-partitioning error as the reason for poor reproduction of individual fluxes in the DL case.

As illustrated in Fig. 10, friction velocity is again overestimated by both OU-LES and WRF model predictions. Although the time evolution is captured closely in general terms, the predicted values of u_* are sometimes 2 times the observed ones. Differences among WRF model predictions of u_* with different schemes are generally small, with the ACM scheme reproducing values that are slightly closer to observations than are those of the YSU and MYJ schemes. The turbulence temperature scale produced by the WRF model is in generally good agreement with OU-LES and observational data, although during the second half of the day the modeled θ_* magnitudes are slightly underestimated. This underestimation is connected with the previously noted overprediction of friction velocity by the WRF model during the same section of the day.

Figure 11 shows that, although the WRF model consistently underestimates the CBL depth, its predicted evolution pattern follows the CBL depth timeline from the OU-LES closely. For the most part of the day, little or no difference is observed among the predictions using different schemes. The evolution of the stability parameter becomes problematic starting at approximately 1800 UTC. Here, WRF model predictions, OU-LES results, and observational data all diverge, with WRF model values of $-z_i/L$ being smaller than the ones predicted by OU-LES and than are indicated by observations. This again highlights the sensitivity of the stability parameter to the value of friction velocity, which is severely overestimated by the WRF model throughout the whole day of 8 June 2007.

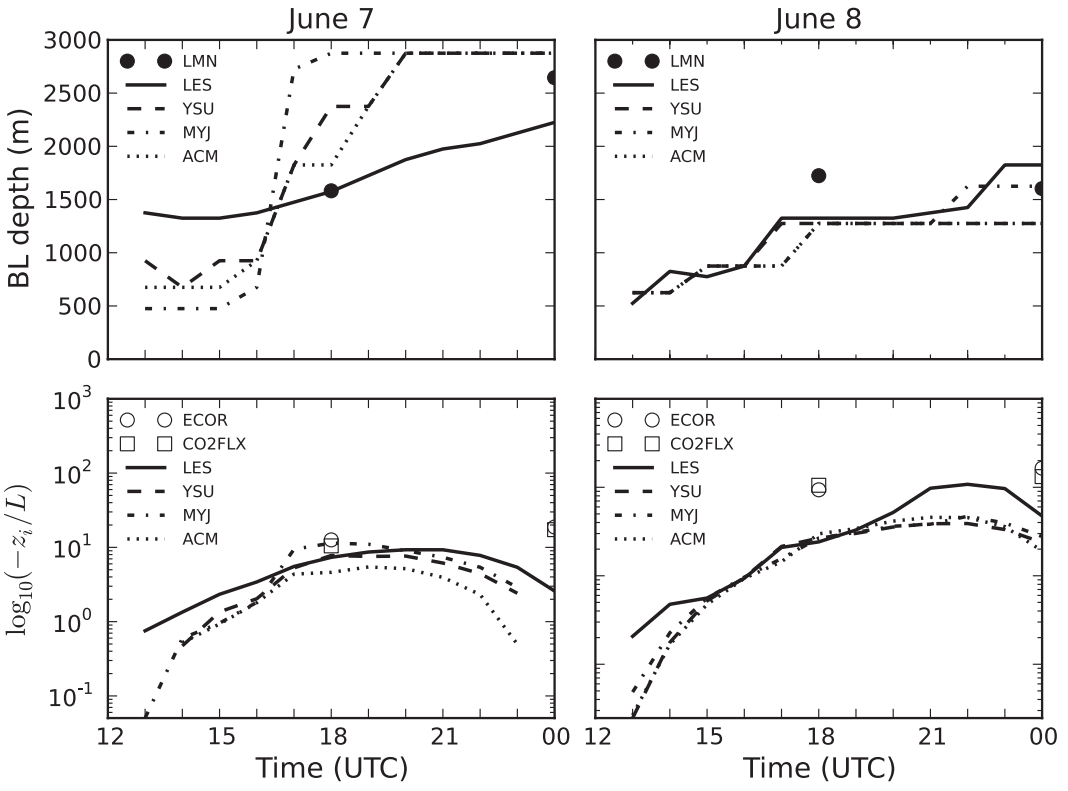

FIG. 11. Evolution of (top) z_i and (bottom) stability parameter $-z_i/L$ predicted by the WRF model with different parameterization schemes for (left) 7 Jun 2007 (DL case) and (right) 8 Jun 2007 (CF case). Observational (LMN, ECOR, and CO2FLX) and LES data are also shown (for unstable conditions only).

5. Conclusions

Previous studies have suggested that, for scale ranges characteristic of CBL processes, the validity of commonly employed subgrid turbulence parameterization is questionable for model applications with grid spacing in the 1–4-km range. Although this feature of model performance is not novel, our goal was to demonstrate and quantify implications of running the WRF model with such grid spacings for prediction of near-surface turbulent flow parameters that are crucial for many practical applications.

The sensitivity of WRF model predictions of CBL turbulence parameters to commonly employed SL/PBL parameterizations was investigated in conjunction with differing grid spacing. Results from the WRF model were compared with observational data and OU-LES output for two cases of a dry CBL over the SGP of the United States. Horizontal grid spacing variations within the range from 1 to 4 km led to minimal differences in the majority of predicted boundary layer flow parameters. When notable differences were observed, the sensitivity tendencies were inconsistent. In our opinion, the differences associated with grid spacing refinement do not warrant the 16-fold increase in computational overhead when moving from a 4-km mesh to a 1-km mesh over the same geographic domain for conditions considered in this study. This conclusion has been also reached in other studies, as mentioned previously, but it may not apply to regions for which more complex surface conditions exist. It may seem obvious that the homogeneous terrain in central Oklahoma would always yield such insensitivity to grid spacing for this particular scale range, but the complex turbulence properties in the CBL coupled with the uncertain breakdown of inherent assumptions adopted in turbulence modeling within the considered scale range give a reason to believe that such a study was warranted. We feel that a more reasonable use of computational expense would be to expand the horizontal size of the domain or to increase the number of vertical levels in the model.

For the WRF model configurations using 4-km grid spacing, the nonlocal schemes (YSU and ACM) were consistently predicting a drier CBL than did the local scheme (MYJ). The potential temperature differences among model outputs using different schemes were

generally small. The nonlocal schemes usually resulted in smaller discrepancies with observations early in the simulation period than did the MYJ scheme. For the DL case, wind speeds were underestimated by the WRF model, whereas for the CF case they were overestimated. The local scheme more closely reproduced wind magnitudes and time evolution than did the nonlocal schemes for the DL case, while the opposite was true for the CF case. Differences in the wind direction were generally inconsequential. In our opinion, nonlocal SL/PBL schemes better reproduce meteorological features in turbulent flow during conditions typical of a dry CBL considered in this study as compared with the local scheme. There are limitations of using any of the considered schemes within the studied scale range of CBL turbulent motions, however, especially in the presence of strong convection.

In the two studied CBL cases, the surface flux predictions by the YSU scheme were routinely closest to the observed flux values and the ACM scheme predictions were farthest away. An apparent partitioning error was discovered in the predictions of heat fluxes for the DL case, for which the surface sensible heat fluxes and surface latent heat fluxes were drastically underestimated and overestimated, respectively. The behavior of the total heat flux (sensible and latent fluxes added together) across both cases lends support to these proposed reasons for the flux discrepancies. It was also shown that values from two separate instruments at the same location could vary by a factor of 2, however. This pointed to the possibility of instrumentation error. Another issue of determining the flux values is associated with the inherent problem of comparing domain-averaged values with the data from a single-point observation. While no clear answer was found as to how to interpret the differences, their mere existence highlights potential problems that a model user must consider in this particular framework.

The local scheme was closer to observations than the nonlocal schemes were in predictions of the near-surface turbulence parameters for the DL case, whereas the nonlocal schemes were closer for the CF case. In both cases, the friction velocity was overestimated by all tested WRF model SL/PBL schemes, as well as by OU-LES, and the turbulence temperature scale was systematically underestimated. The WRF model was overzealous in the mechanical production of turbulence and was derelict in buoyancy production, which is potentially consistent with the apparent breakdown of the fundamental assumptions of the employed SL/PBL schemes within the ranges of scales of motion corresponding to the investigated grid spacings. As a result, the stability parameter was underestimated by the WRF model (it was indicative of less convective conditions in the boundary layer) in comparison with OU-LES and observational data. The WRF model with all SL/PBL schemes was generally closer to observations when convective (buoyant) forcing was less intense, as may be concluded from the CBL-depth estimates and surface sensible heat flux values.

Although the reader is left without a definitive recommendation for the use of specific schemes in the WRF model, we believe there is value in showing that under the conditions considered in our paper one cannot go horribly wrong in choosing particular parameterizations. It was demonstrated that the nonlocal schemes were slightly closer to observations in most instances but that the local scheme was not far off and was even closer to observations in certain situations. Given the physics accounted for in the nonlocal schemes, it is interesting to note that the local scheme performed as admirably as it did with the conditions present in the study. Further studies would be needed to draw more particular conclusions regarding performance of different turbulence schemes in the WRF model. Nonetheless, the findings presented here offer a starting point for designing a model study aimed at the prediction of near-surface turbulence parameters.

REFERENCES

Benjamin, S. G., K. J. Brundage, and L. L. Morone, 1994: Implementation of the Rapid Update Cycle. Part I: Analysis/model description. NOAA/NWS Tech. Procedures Bull. 416, 16 pp.

Botnick, A. M., and E. Fedorovich, 2008: Large eddy simulation of atmospheric convective boundary layer with realistic environmental forcings. *Quality and Reliability of Large-Eddy Simulations,* J. Meyers et al., Eds., Springer, 193–204.

Chen, F., and J. Dudhia, 2001: Coupling an advanced land surface–hydrology model with the Penn State–NCAR MM5 modeling system. Part I: Model description and implementation. *Mon. Wea. Rev.,* **129,** 569–585.

Conzemius, R. J., and E. Fedorovich, 2008: A case study of convective boundary layer development during IHOP 2002: Numerical simulations compared to observations. *Mon. Wea. Rev.,* **136,** 2305–2320.

Cook, D. R., and M. S. Pekour, 2008: Eddy correlation flux measurement systems handbook. DOE Tech. Rep. DOE/SC-ARM/TR-05, 20 pp.

Deardorff, J. W., 1970: Convective velocity and temperature scales for the unstable planetary boundary layer and for Rayleigh convection. *J. Atmos. Sci.,* **27,** 1211–1213.

——, 1972: Numerical investigation of neutral and unstable planetary boundary layers. *J. Atmos. Sci.,* **29,** 91–115.

——, 1980: Stratocumulus-capped mixed layers derived from a three-dimensional model. *Bound.-Layer Meteor.,* **18,** 495–527.

Dudhia, J., 1989: Numerical study of convection observed during the winter monsoon experiment using a two-dimensional model. *J. Atmos. Sci.,* **46,** 3077–3107.

Dyer, A. J., and B. B. Hicks, 1970: Flux-gradient relationships in the constant flux layer. *Quart. J. Roy. Meteor. Soc.,* **96,** 715–721.

Fedorovich, E., R. Conzemius, and D. Mironov, 2004a: Convective entrainment into a shear-free, linearly stratified atmosphere: Bulk models reevaluated through large eddy simulations. *J. Atmos. Sci.,* **61,** 281–295.

——, and Coauthors, 2004b: Entrainment into sheared convective boundary layers as predicted by different large eddy simulation codes. Preprints, *16th Symp. on Boundary Layers and Turbulence,* Portland, ME, Amer. Meteor. Soc., P4.7. [Available online at http://ams.confex.com/ams/pdfpapers/78656.pdf.]

Fischer, M. L., 2005: Carbon dioxide flux measurement systems handbook. DOE Tech. Rep. ARM TR-048, 15 pp.

Holtslag, A. A. M., and P. G. Duynkerke, Eds., 1998: *Clear and Cloudy Boundary Layers*. Royal Netherlands Academy of Arts and Sciences, 372 pp.

Hong, S., J. Dudhia, and S. H. Chen, 2004: A revised approach to ice microphysical processes for the bulk parameterization of clouds and precipitation. *Mon. Wea. Rev.,* **132,** 103–120.

——, Y. Noh, and J. Dudhia, 2006: A new vertical diffusion package with an explicit treatment of entrainment processes. *Mon. Wea. Rev.,* **134,** 2318–2341.

Janjić, Z. I., 1990: The step-mountain coordinate: Physical package. *Mon. Wea. Rev.,* **118,** 1429–1443.

——, 1996: The surface layer in the NCEP Eta Model. Preprints, *11th Conf. on Numerical Weather Prediction,* Norfolk, VA, Amer. Meteor. Soc., 354–355.

——, 2001: Nonsingular implementation of the Mellor–Yamada level 2.5 scheme in the NCEP Meso Model. NCEP Tech. Rep. 437, 61 pp.

Kain, J. S., and Coauthors, 2008: Some practical considerations regarding horizontal resolution in the first generation of operational convection-allowing NWP. *Wea. Forecasting,* **23,** 931–952.

Mason, P. J., 1989: Large-eddy simulation of the convective atmospheric boundary layer. *J. Atmos. Sci.,* **46,** 1492–1516.

Mellor, G. L., and T. Yamada, 1982: Development of a turbulence closure model for geophysical fluid problems. *Rev. Geophys. Space Phys.,* **20,** 851–875.

Mesinger, F., and Coauthors, 2004: NCEP North American Regional Reanalysis. Preprints, *15th Symp. on Global Change and Climate Variations,* Seattle, WA, Amer. Meteor. Soc., P1.1. [Available online at http://ams.confex.com/ams/pdfpapers/72502.pdf.]

Mlawer, E. J., S. J. Taubman, P. D. Brown, M. J. Iacono, and S. A. Clough, 1997: Radiative transfer for inhomogeneous atmospheres: RRTM, a validated correlated-*k* model for the longwave. *J. Geophys. Res.,* **102,** 16 663–16 682.

Moeng, C.-H., 1984: A large-eddy simulation for the study of planetary boundary layer turbulence. *J. Atmos. Sci.,* **41,** 2052–2062.

Monin, A. S., and A. M. Obukhov, 1954: Basic laws of turbulent mixing in the surface layer of the atmosphere. *Tr. Akad. Nauk SSSR Geophiz. Inst.,* **24,** 163–187.

Paulson, C. A., 1970: The mathematical representation of wind speed and temperature profiles in the unstable atmospheric surface layer. *J. Appl. Meteor.,* **9,** 857–861.

Pleim, J. E., 2006: A simple, efficient solution of flux-profile relationships in the atmospheric surface layer. *J. Appl. Meteor. Climatol.,* **45,** 341–347.

——, 2007: A combined local and nonlocal closure model for the atmospheric boundary layer. Part I: Model description and testing. *J. Appl. Meteor. Climatol.,* **46,** 1383–1395.

——, and J. S. Chang, 1992: A non-local closure model for vertical mixing in the convective boundary layer. *Atmos. Environ.,* **26A,** 965–981.

——, and A. Xiu, 1995: Development and testing of a surface flux and planetary boundary layer model for application in mesoscale models. *J. Appl. Meteor.,* **34,** 16–32.

Ritsche, M. T., 2008: Surface meteorological observation system handbook. DOE Tech. Rep. DOE/SC-ARM/TR-031, 31 pp.

Schmidt, H., and U. Schumann, 1989: Coherent structure of the convective boundary layer derived from large-eddy simulations. *J. Fluid Mech.,* **200,** 511–562.

Schwartz, C. S., and Coauthors, 2009: Next-day convection-allowing WRF model guidance: A second look at 2-km versus 4-km grid spacing. *Mon. Wea. Rev.,* **137,** 3351–3372.

Skamarock, W. C., J. B. Klemp, J. Dudhia, D. O. Gill, D. M. Barker, W. Wang, and J. G. Powers, 2008: A description of the Advanced Research WRF version 3. NCAR Tech. Note NCAR/TN-475+STR, 113 pp. [Available online at http://www.mmm.ucar.edu/wrf/users/docs/arw_v3.pdf.]

Smagorinsky, J., 1963: General circulation experiments with the primitive equations. *Mon. Wea. Rev.,* **91,** 99–164.

Stull, R. B., 1988: *An Introduction to Boundary Layer Meteorology*. 1st ed. Springer, 666 pp.

Wyngaard, J. C., 2004: Toward numerical modeling in the ''terra incognita.'' *J. Atmos. Sci.,* **61,** 1816–1826.

Xiu, A., and J. E. Pleim, 2001: Development of a land surface model. Part I: Application in a mesoscale meteorological model. *J. Appl. Meteor.,* **40,** 192–209.